J. Fluid Mech. (1990), *vol.* 221, *pp.* 485–509
Printed in Great Britain

Radial spreading of viscous–gravity currents with solidifying crust

By JONATHAN H. FINK[1,2] AND ROSS W. GRIFFITHS[1]

[1] Research School of Earth Sciences, Australian National University, Canberra, Australia
[2] Geology Department, Arizona State University, Tempe, AZ 85287, USA

(Received 20 July 1989 and in revised form 24 May 1990)

We have investigated the effect of a solidifying crust on the dynamics and surface morphology of radial viscous–gravity currents. Liquid polyethylene glycol was admitted into the base of a tank filled with cold sucrose solution maintained at a temperature below the wax freezing point. As the radial current advanced away from the inlet, its surface solidified and deformed through a combination of folding and fracturing. For the warmest experiments, during which solidification did not occur, the radius of the current increased in proportion to the square root of time, as demonstrated both experimentally and theoretically for isothermal viscous fluids by Huppert (1982). When cooling was sufficiently rapid, solid crust formed and caused the spreading rate to decrease. A cooling model combining conduction in the wax with convection in the sucrose solution predicts the distance from the source at which the solid crust first appeared.

Progressively colder experiments revealed a sequence of surface morphologies which resembled features observed on cooling lava flows and lava lakes. Flows in which crust formed very slowly developed marginal levees which contained and channelled the main portion of the current. Colder flows with more rapid crust growth formed regularly spaced surface folds, multi-armed rift structures complete with shear offsets, and bulbous lobate forms similar to pillow lavas seen under the ocean. The same transitions between modes of surface deformation were also generated by keeping the ambient water temperature constant and decreasing the extrusion rate. This demonstration that surfaces can exhibit a well-defined sequence of morphologies which depend on the underlying flow conditions offers the prospect of more successful interpretation of natural lava flows.

1. Introduction

If a fluid of high viscosity is poured rapidly onto a flat surface, it will pile up and spread radially with a velocity controlled by gravitational and viscous forces. Such viscous–gravity currents have been investigated both theoretically and experimentally because they are good analogues for numerous geophysical phenomena including the spread of oil slicks (Hoult 1972), the intrusion of salt water into fresh water (Didden & Maxworthy 1982), and the growth of lava domes (Huppert *et al.* 1982). Application of these purely viscous models to lava flows has been limited, however, because most lavas are covered by a solidified crust which thickens with time. Such a cooled surface can raise the bulk viscosity of the current, impart a yield strength, increase stresses exerted on the liquid and retard the radial velocity. Deformation of this crust in response to stresses applied by the underlying viscous

flow produces the characteristic morphologic features used by geologists to interpret the rheology and emplacement history of lava flows.

Most theoretical models of lava flow processes attempt to explain the overall dimensions of flows, rather than their surface appearance. Flow length and areal distribution have been related to such variables as total erupted volume (Malin 1980), volume flow rate (Walker 1973; Wadge 1978), viscosity (Huppert *et al.* 1982; Baloga 1987), and cooling rate (Crisp & Baloga 1990; Pinkerton 1987; Pieri & Baloga 1986). The surface morphology and structure of flows have received less attention, with selected studies focusing on the formation of individual features. Marginal levees have been used as indicators of isothermal yield strength (Hulme 1974). Regularly spaced surface ridges and buoyant zones of pumice have been related to surface and interior viscosities (Fink & Fletcher, 1978; Fink 1980*a*) and to density gradients in the flow (Fink 1980*b*, 1983; Baum *et al.* 1989). Spreading cracks on submarine pillow lavas (Moore & Lockwood 1978) and paired, outwardly convex fractures on the surfaces of silicic lava domes (Anderson & Fink 1990), have both been used to help determine emplacement temperatures and thermal gradients. However, to date no comprehensive models that address the formation of more than one or two of these features have appeared.

Most laboratory simulations of lava flows have similarly centred on their large-scale dynamics and geometry. These studies have primarily used isothermal Bingham plastics such as kaolin slurries (e.g. Hulme 1974; Blake 1990) or temperature-dependent Newtonian fluids such as polyethylene glycol (PEG) (e.g. Hodgson 1969; Greeley & Womer 1981; Hallworth, Huppert & Sparks 1987) to constrain factors controlling the spreading rate, branching patterns, and total flow length. Among the simplest laboratory configurations were those of Huppert (1982), who used isothermal Newtonian silicone oils to model the radial spread of viscous gravity currents, and Blake (1990) who substituted kaolin into Huppert's (1982) set-up to examine the effect of yield strength on spreading rate. Although earlier workers had used temperature-dependent materials such as PEG, Hallworth *et al.* (1987) were the first to inject it under water to minimize surface tension effects and increase cooling rates to realistic values. While the study focused on the effects of slope and extrusion rate on the development of branching patterns and three-dimensional flow fields, their experimental flows reproduced several realistic morphologic features such as levees and lava tubes.

The present study uses laboratory simulations and theoretical arguments to show that a sequence of lava flow structures including marginal levees, surface corrugations oriented normal to the flow direction, surface fractures, and bulbous pillows are related to crustal growth rates. It is based on an experimental investigation of the spread of viscous–gravity currents with solidifying crust. We have conducted a series of 72 experiments in which polyethylene glycol maintained at a temperature just above its freezing point was injected into the bottom of a tank containing sucrose solution held at a lower temperature. When the bath temperature was low enough, solid crust developed on the surface of the spreading flow. Subsequent compression, extension, and shear of the flow surface resulted in a range of morphologic features similar to those seen on natural lava flows. Flow-front position, radial velocity, and strain rate also were determined as functions of time.

We begin with an analysis which compares the rate at which heat is carried away from the surface of a viscous fluid by turbulent convection in the overlying water to the rate at which heat is advected laterally by the viscous flow. The analysis predicts the distance from a vent at which surface solidification will begin, and we argue that

the morphology of a flow will be controlled by the rate of solidification of crust. Next we present our experimental results and compare them with equivalent data obtained by Huppert (1982) for the axisymmetric propagation of isothermal Newtonian fluids, and by Blake (1990) for the spread of isothermal Bingham plastics. Increasing deviation from the linear viscous results for progressively colder experiments is related to the cooling model. The conditions necessary to form various surface morphologies are outlined, and application to the interpretation of lava flows is discussed.

2. Viscous flows with surface cooling and solidification

2.1. *Global parameters*

Previous studies have considered viscous gravity currents in which there are no temperature or viscosity gradients, and no mechanically distinct crustal layer. One of the simplest flows, and possibly the most instructive, is the case of a constant volume flux issuing from a point source on to a planar surface (Huppert 1982). Here we assume that the environment has a viscosity much smaller than that of the source fluid and conditions are such that there is a simple balance between buoyancy and viscous forces. This flow is fully described by four variables: the angle β of the plane to the horizontal, the fluid kinematic viscosity ν, the volume flow rate Q and the reduced gravity $g' = g\Delta\rho/\rho$ (where $\Delta\rho$ is the density difference between the source fluid and environment and ρ is the density of the source fluid). Huppert (1982) presents a similarity solution to the axisymmetric radial flow on a horizontal plane ($\beta = 0$) in which the depth H of the fluid and the velocity U_n of the leading edge of the spreading current scale as

$$H \sim \left(\frac{Q\nu}{g'}\right)^{\frac{1}{4}}, \quad U_n \sim \left(\frac{g'Q^3}{\nu}\right)^{\frac{1}{8}} t^{-\frac{1}{2}}. \tag{1}$$

The flow can also be described in terms of a global (time-invariant) velocity scale $U \sim (g'Q/\nu)^{\frac{1}{2}}$.

Cooling and solidification of the surface of the viscous fluid may remove the self-similarity of the flow. It also involves a number of additional physical variables. Consider a viscous liquid (such as lava or wax but which, for convenience, we shall refer to as lava) extruding from a vent at a temperature T_l and spreading over a rigid plane beneath air or water at an ambient temperature T_a. The variables are β, g', Q, ν, T_a, T_l, as well as other physical properties of both the lava and the ambient fluid, namely the solidification temperature(s) T_s, the expansion coefficients (α and α_a), the diffusion coefficients for heat (κ and κ_a), the viscosity of the ambient fluid (ν_a), the emissivity of the lava surface (when radiation is significant), and the temperature-dependent rheologies of the lava and its solid crust. Latent heat of solidification is negligible in lava crust, where quenching forms a glass, and we shall assume that the laboratory wax also solidifies without crystallization. The properties of the lava and its crust directly determine the mechanics of the flow, while those of the ambient fluid enter only through their influence on the heat transport from the lava surface.

The dimensionless parameters necessary to describe the system can be established by physical arguments. One variable of primary importance is the amount of cooling

necessary for solidification. This can be measured in terms of the overall temperature difference $\Delta T = T_l - T_a$ which causes the cooling, and we form the parameter

$$\Theta_s = \frac{T_s - T_a}{T_l - T_a}. \tag{2}$$

No solidification is possible if $\Theta_s < 0$, and Θ_s must be less than 1 for the lava to be liquid at the source. For Θ_s small and positive no solidification is expected because the surface is unlikely to reach its freezing point. For Θ_s close to 1 a solid crust will form rapidly and will tend to develop close to the vent.

A second factor influencing the presence or otherwise of crust and the rate of solidification is the rate of radial advection of the lava surface (and of heat) compared with the rate of cooling of the lava. Assuming that the heat transfer within the lava is controlled predominantly by conduction of heat (an assumption that is verified below) a Péclet number Pe can be formed as a ratio of the global lateral velocity scale U and the diffusion velocity κ/H (where H is again the depth scale (1)):

$$Pe = \frac{UH}{\kappa} = \frac{1}{\kappa}\left(\frac{g'Q^3}{\nu}\right)^{\frac{1}{4}}. \tag{3}$$

This study is concerned only with flows for which the depth of the thermal boundary layer in the lava is much less than the depth of the lava ($Pe \gg 1$). However, the greater the value of Pe is, the smaller the heat loss from the surface and the thinner the boundary layer at any given distance from the vent. Alternatively, the larger Pe is, the farther the lava surface moves before it reaches its solidification temperature. Note that we have already demanded that the fluid has a large Prandtl number by requiring a thin thermal boundary layer along with the viscous–buoyancy balance.

The Péclet number (3) and the amount of cooling required before solidification begins (Θ_s) are not the only parameters that determine the rate of crust growth. The Péclet number measures the rate of conductive heat transport toward the surface compared with the rate of advection of heat, and the thickness of the thermal boundary layer compared with the lava depth. However, the conductive heat flux is depth-dependent and the boundary layer cools with time. The rate at which the lava surface temperature decreases, hence the distance from the vent at which solidification begins, is influenced by the magnitude of the radiative or convective surface flux compared with the conductive flux in the lava. Thus we require a dimensionless parameter, call it Ψ, which gives the ratio of surface heat flux to the conductive flux or, more usefully, the time taken to reduce the contact temperature to the freezing point compared to the time for lateral advection of fluid through a distance H. Because rapid cooling under laboratory conditions is most conveniently achieved by injecting a viscous fluid into a chilled water bath we shall concentrate on the case of convective cooling and present below a model that gives the appropriate form of the surface cooling parameter Ψ.

Two additional parameters influencing the flow are the slope β of the surface on which the current spreads and the mechanical properties of the crust. The slope tends to orient the motion towards the downslope direction, elongating the shape of the advancing front. Hence the thickness of crust and the stresses exerted on that crust vary with direction from the source. Whatever the slope, the effects of crust on the flow and the deformation or fracturing of the crust in response to the flow both will depend upon the compressive, tensional and shear strengths of the solid, and perhaps

a viscosity as well. Each of these strengths, denoted by σ, can be compared with the applied viscous stresses (or with the buoyancy force), giving parameters of the form

$$\Sigma = \frac{\sigma H}{\rho \nu U} = \frac{\sigma}{\rho}(g'^3 Q \nu)^{-\frac{1}{4}}. \tag{4}$$

Along with the temperature parameter Θ_s and Péclet number Pe, the strength parameter Σ may potentially influence the rate of spreading of the front and the type and position of deformation structures occurring on the crust. For example, a stronger crust could imply that transverse folds, which are due to buckling of the crust under a compressive (radial) stress, will either occur closer to the vent, where the crust is thinner, or not at all. Advance of the front will be slowed by a stronger crust if spreading relies on fracturing of the crust under pressures determined by the depth of the flow. On the other hand, the magnitude of the tensile strength may be of no significance if fracturing is not required for spreading, and this may be the case whenever existing 'weak' zones are maintained by flow divergence (as at a rift) or by flushing (as in a 'lava tube'). Furthermore, estimates of the tensile strengths of lava and PEG wax imply $\Sigma \sim 10^2$ and $\Sigma \sim 10^4$, respectively. Thus $\Sigma \gg 1$ in both cases. Hence buoyancy or viscous stresses cannot fracture crust except where it is very thin. Likewise, buckling will be limited to a region where a thin crust is slowly forming.

A further complication arises if there is heat flow from the lava to the underlying surface. Solidification may then occur at the base of the flow. The effects of this, however, are expected to be small so long as only a small thickness of solidified lava is formed. The rigid base supporting the viscous stresses is simply displaced upward by a small increment, and the depth of the flow and the driving buoyancy force reduced accordingly.

2.2. *Surface cooling by a convective flux*

In order to evaluate the effects of cooling on the radial spreading of viscous–gravity currents we first need to calculate how the surface temperature of the liquid decreases with distance from the vent and where solidification will begin. On contact with colder water the surface of the lava immediately begins to cool by conduction. A cold thermal boundary layer of thickness $\delta \approx 2(\kappa t)^{\frac{1}{2}}$ develops in the lava as it moves away from the vent. Although more dense than the bulk of the lava, this cold boundary layer remains stable to the onset of convection until the Rayleigh number $R_b = g\alpha \Delta T \delta^3/\kappa\nu$, based on the depth δ, exceeds a critical value of order 10^3. This implies that the onset of convection requires a time of order 10^3 s in the case of the PEG wax used in the laboratory and at least 10^5 s in lavas. However, we are only interested in the early development of a solid crust, which in both cases takes a much shorter time. We can therefore assume that heat transfer within the lava (and its crust) is by conduction alone.

Heat transfer in the water, on the other hand, will be largely dominated by a flux due to turbulent convection. This is because the growth of an unstable conductive boundary layer in the much less viscous water requires only a very short time (of order 10 s in our laboratory experiments or less than 1 s above lavas) and because the Rayleigh number based on the depth of water is (by assumption) greater than 10^6. Thus the water above the lava is in turbulent convection almost as soon as the intrusion is initiated. Above a small vent (or any other centre of lateral spreading) there is a continuous supply of hot lava to the lava–water interface, and so the

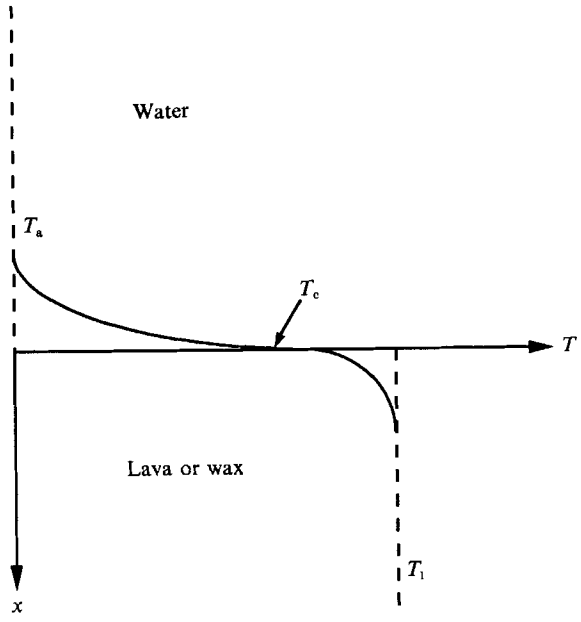

FIGURE 1. Initial temperature distribution assumed in the cooling analysis (broken line), and schematic of a later temperature profile (solid line). T_c = contact temperature.

contact temperature (T_c) near the vent is closely approximated by the vent or interior lava temperature. The intermittent conductive–convective boundary layer in the water must match this contact temperature to the ambient water temperature. As the lava moves away from the vent the contact temperature will decrease and eventually approach the water temperature.

We apply a one-dimensional cooling model to the spreading lava by placing ourselves in the frame of reference moving with the velocity of the lava surface. The resulting temperature distribution is sketched in figure 1. Conductive heat transfer in the lava is matched to the heat flux $F(t)$ from its surface, with the initial condition

$$T = T_l, \quad t = 0, \quad x \geqslant 0. \tag{5}$$

The surface flux is taken as that due to turbulent convection and is given by

$$F = \gamma \rho_a c_a \left(\frac{g\alpha_a \kappa_a^2}{\nu_a}\right)^{\frac{1}{3}} (T_c - T_a)^{\frac{4}{3}} \tag{6}$$

(Turner 1973), where T_c is the contact temperature, α_a, κ_a, ν_a, ρ_a and c_a are the physical properties of the water and γ is a dimensionless constant whose empirical value is close to 0.1. This flux should be accurate at times greater than the intermittency timescale for convection in the water. However, it will only roughly approximate the heat loss over cooling times less than 10 s in the laboratory. At such small times there may be both temporal and spatial variations in the extent of surface cooling as a result of convective motions and an unsteady thermal boundary layer in the water.

The general solution for the temperature profile resulting from a time-dependent surface flux $F(t)$ is given by Carslaw & Jaeger (1959, p. 76, eq. 9) in the form of an integral equation. That solution can be combined with the expression (6) for the

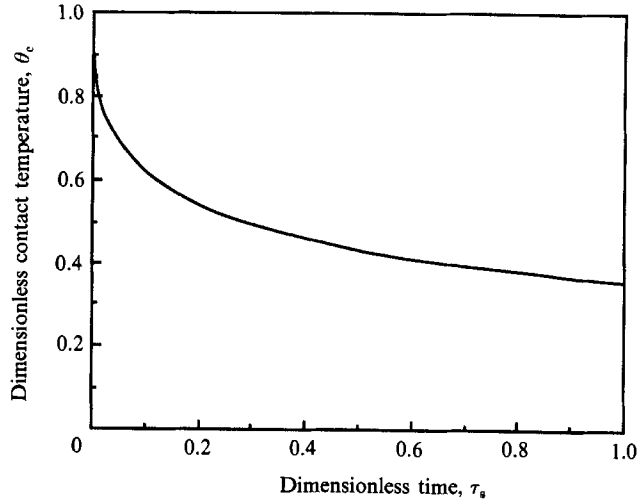

FIGURE 2. The predicted variation of the contact temperature with time, modified from Huppert & Sparks (1988). See text for definitions of dimensionless contact temperature and time.

surface flux and gives an equation for the contact temperature as a function of time. Defining a dimensionless contact temperature and time as

$$\theta_c = \frac{T_c - T_a}{\Delta T} \tag{7}$$

and

$$\tau = \frac{t}{\lambda}, \tag{8a}$$

where

$$\lambda = \left(\frac{\rho c}{\rho_a c_a}\right)^2 \frac{\pi}{\gamma^2} \left(\frac{\nu_a}{g\alpha_a \Delta T}\right)^{\frac{2}{3}} \frac{\kappa}{\kappa_a^{\frac{4}{3}}}, \tag{8b}$$

the equation for the contact temperature reduces to

$$\theta_c = 1 - \int_0^\tau \left\{\frac{[\theta_c(\zeta)]^{\frac{4}{3}}}{(\tau-\zeta)^{\frac{1}{2}}}\right\} d\zeta. \tag{9}$$

The timescale λ in (8) is simply that over which T_c decreases from the vent temperature towards T_a. Equation (9) is to be solved for the initial condition $\theta_c(0) = 1$. As $\tau \to \infty$ the contact temperature approaches the water temperature ($\theta_c \to 0$). Huppert & Sparks (1988, Appendix) have used this solution (but with a slightly different non-dimensionalization) to calculate the surface temperature of the roof of a magma chamber in contact with a hot, turbulently convecting magma. We make use of their calculation here, but concentrate on the behaviour at small values of τ. The numerical solution of (9) (Huppert & Sparks, 1988, figure 15) is reproduced, in terms of our variables for small values of τ, in figure 2. Note that the dependence of the convective flux on the contact temperature implies that the flux decreases in time and this causes θ_c to decrease more slowly than the relatively simple $1-\tau^{\frac{1}{2}}$ dependence predicted by the same model but with a constant surface flux (Carslaw & Jaeger 1959, p. 75).

The solution in figure 2 can be used to predict the time elapsed before the lava surface reaches the solidification temperature: we expect the lava surface to be solid if $\theta_c < \Theta_s$. Equivalently, there is a dimensionless time τ_s such that $\theta_c = \Theta_s$ at $\tau = \tau_s$

and the surface solidifies when $\tau > \tau_s$. Thus, knowing Θ_s we can find τ_s and, from (8), the actual time (t_s) to the beginning of solidification.

Our next step is to define and evaluate the dimensionless parameter Ψ which, as discussed earlier, is the ratio of the time t_s for the lava surface to reach its solidification temperature to a timescale t_A for horizontal advection through one current depth. Using the depth H given in (1) and the global velocity scale U, $t_A = (\nu^3/g'^3Q)^{\frac{1}{4}}$. After combining this expression with (3) using (8) we obtain

$$\Psi = \Pi\tau_s(\Theta_s), \tag{10}$$

where Π is a modified Péclet number

$$\Pi = \left(\frac{g'}{\nu}\right)^{\frac{2}{3}}\kappa^{\frac{1}{3}}\lambda Pe^{\frac{1}{3}} = \left(\frac{\rho c}{\rho_a c_a}\right)^2 \frac{\pi}{\gamma^2}\left(\frac{\Delta\rho}{\rho\alpha_a \Delta T}\right)^{\frac{2}{3}}\left(\frac{\nu_a}{\nu}\right)^{\frac{2}{3}}\left(\frac{\kappa}{\kappa_a}\right)^{\frac{4}{3}} Pe^{\frac{1}{3}}. \tag{11}$$

When the above cooling problem is applied to a spreading gravity current, the solidification time corresponds to a distance travelled, r_s. There will be no crust at distances less than r_s from the vent, at least during the early stages of the axisymmetric flow. Some solid crust will appear at larger radii, although not all of the surface at $r > r_s$ will be crusted since radial flow involves azimuthal stretching of the surface, and stretching need not remain axisymmetric once some solid has developed. If the spreading was two-dimensional, as if from a line source, the distance r_s normalized by the depth H would be equal to Ψ and could be evaluated from (10). For spreading from a point source, however, the radial velocity decays with distance from the source approximately as r^{-1} (assuming constant depth). Hence the velocities of fluid parcels decrease approximately as $t^{-\frac{1}{2}}$. Integrating the velocity scale in (1) over the solidification time t_s gives

$$r_s \approx \left(\frac{g'Q^3}{\nu}\right)^{\frac{1}{8}} t_s^{\frac{1}{2}} = (Pe\,\kappa t_s)^{\frac{1}{2}}. \tag{12}$$

Normalizing the radius by the flow depth H, (1), eliminating Q using (3) and non-dimensionalizing the time according to (8) we obtain

$$\frac{r_s}{H} \approx (\Pi\tau_s)^{\frac{1}{2}} = \Psi^{\frac{1}{2}}. \tag{13}$$

In summary, physical considerations and the above cooling model indicate that the primary parameter controlling the solidification of crust is Ψ, the dimensionless time take for the surface temperature of the viscous fluid to reach the solidification temperature. The hypothesis that we aim to test in laboratory experiments is that it is primarily this solidification time, or the distance from the vent at which crust begins to form, that determines the character of the flow and the way in which the current continues to spread. A further dependence on the rheology of the crust (particularly its resistance to buckling and fracture) has not been tested. Because Ψ is usefully broken down into two distinct contributions, that from Θ_s and that from the Péclet number Π (equation (10)), the experimental flows will also be examined in terms of these two parameters.

3. Experimental procedure

Polyethylene glycol (PEG) is a commercially available water-soluble wax which has been used to model volcanic processes by several previous investigators (e.g. Greeley & Womer 1981; Park 1981; Hallworth *et al.* 1987). PEG comes in several

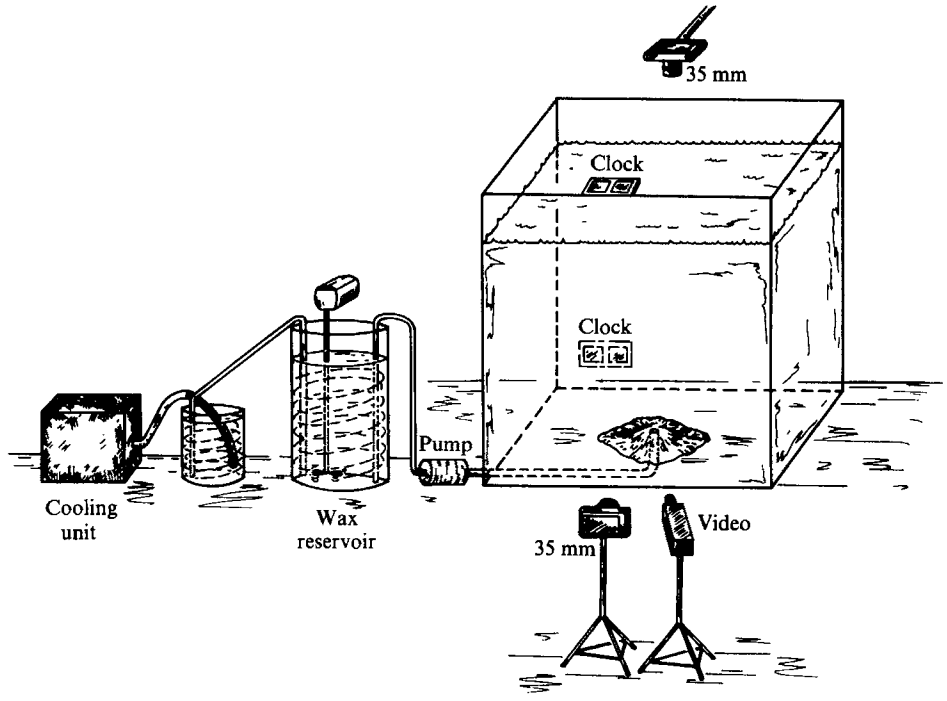

FIGURE 3. Experimental set-up for constant-extrusion-rate runs nos. 25–54. Sucrose solution in the tank is maintained at constant temperature by an additional cooling coil and stirrer (not shown) which are removed just prior to the start of an experiment.

grades which differ in molecular weight, freezing temperature, solubility in water, and other physical properties. We selected PEG 600 because it is liquid at room temperature and freezes over a range of temperatures easy to obtain in the laboratory. Following Hallworth *et al.* (1987), we designed our experiments so that wax would be injected into a tank of relatively cold liquid, rather than air, in order to reduce the influence of surface tension and to increase the cooling rate. We used sucrose solution rather than water to reduce the density contrast and to lower the freezing point of the solution.

Three different experimental configurations were used during the course of the investigation. Figure 3 shows the main experimental set-up, used for experiments nos. 25–54 (table 1). A reservoir of blue-dyed PEG was kept at a temperature from 0.5 to 3.5° ($\pm 0.3°$) above its nominal freezing point of 18 °C, using a cooling coil and mechanical stirrer. Sucrose solution was similarly maintained at a temperature between -0.7 and $+14.5$ °C to a depth of approximately 25 cm in a cubic Perspex tank 30 cm on a side. Under the clear base of the tank was a target consisting of concentric circles spaced 2 cm apart and eight equally spaced radial lines. Two synchronized 35 mm cameras were positioned overhead and in front of the tank, and digital clocks were placed in each field of view. A video recorder was located in front of the tank, slightly above horizontal.

The wax was pumped at a constant flow rate through a 1 cm diameter inlet in the centre of the tank base, using a Cole–Parmer peristaltic pump. As the wax spread across the floor of the tank, between 10 and 30 pairs of photographs were taken at varying time intervals. The overhead photographs were later projected onto a digitizing tablet, and eight radii were measured for each frame. The radii from each

Exp	T_l	T_a	$Q_0 \times 10^{-6}$	Slope	Mesh	Type	ρ_l	ρ_a	g'	$\nu_l \times 10^{-4}$	$\nu_a \times 10^{-5}$	λ	$Pe \times 10^3$	$\Pi \times 10^3$	$\Theta_s \times 10^{-1}$	$\tau_s \times 10^{-2}$	t_s	Ψ	r_s/H	r_s
25	19.9	16.2	4.50	0	N	N	1126.5	1113.3	0.115	1.67	3.50	404.7	5.56	2.50	4.86	31.50	127.49	786.0	28.0	25.3
26	20.0	14.5	4.50	0	N	N	1126.4	1113.6	0.111	1.67	3.73	323.9	5.52	1.95	6.36	8.70	28.18	170.0	13.0	11.8
27	20.4	7.0	4.50	0	N	R	1126.1	1115.1	0.095	1.61	5.36	227.0	5.35	1.25	8.21	1.20	2.72	15.0	3.9	3.6
28	19.6	0.0	4.50	0	N	F	1126.8	1116.5	0.089	1.68	7.54	221.0	5.21	1.12	9.18	1.41	3.09	15.7	4.0	3.8
29	19.8	10.5	4.50	0	N	F	1126.6	1114.4	0.106	1.68	4.48	257.6	5.44	1.49	8.06	1.50	3.86	22.3	4.7	4.3
30	19.6	9.5	3.68	0	N	R	1126.8	1114.6	0.106	1.68	4.70	251.9	4.68	1.38	8.42	0.90	2.27	12.4	3.5	3.1
31	19.4	7.5	3.68	0	N	R	1127.0	1115.0	0.104	1.91	5.23	242.1	4.51	1.19	8.82	0.45	1.09	5.3	2.3	2.1
32	19.6	9.6	7.75	0	N	F	1126.8	1114.6	0.106	1.91	4.68	252.6	7.92	1.52	8.40	0.90	2.27	13.7	3.7	4.0
33	19.6	3.5	8.61	0	N	F	1126.8	1115.8	0.095	1.91	6.38	225.7	8.35	1.29	9.01	0.30	0.68	3.9	2.0	2.3
34	19.6	2.5	3.39	0	N	P	1126.8	1116.0	0.094	1.91	6.72	224.2	4.13	1.00	9.06	0.30	0.67	3.0	1.7	1.6
35	21.4	13.6	3.39	0	N	N	1125.1	1113.8	0.099	1.73	3.90	263.6	4.29	1.32	5.64	16.25	42.84	214.0	14.6	12.9
36	21.4	8.5	3.39	0	N	L	1125.1	1114.8	0.090	1.73	4.97	221.1	4.19	1.03	7.36	3.30	7.30	33.9	5.8	5.2
37	21.5	12.7	10.00	0	N	N	1125.0	1114.0	0.096	1.70	4.07	250.1	9.67	1.63	6.02	11.70	29.26	191.0	13.8	16.0
38	21.5	9.8	10.00	0	N	N	1125.0	1114.5	0.091	1.70	4.63	225.1	9.54	1.41	7.01	4.75	10.69	66.9	8.2	9.6
39	21.3	3.0	5.46	0	N	R	1125.2	1115.9	0.081	1.69	6.55	210.2	5.87	1.04	8.20	1.20	2.52	12.4	3.5	3.6
40	19.5	3.6	5.46	0	N	R	1126.9	1115.8	0.096	1.94	6.35	226.8	5.92	1.15	8.43	0.88	2.00	10.1	3.2	3.3
41	19.5	3.1	10.10	0	N	F	1126.9	1115.9	0.095	1.94	6.51	226.0	9.36	1.33	8.48	0.82	1.85	10.9	3.3	4.0
42	19.4	14.2	5.46	0	N	N	1127.0	1113.7	0.115	1.95	3.79	339.9	6.19	1.96	5.38	20.25	68.81	398.0	19.9	19.6
43	19.5	9.5	10.10	0	N	L	1126.9	1114.6	0.106	1.94	4.70	253.6	9.63	1.62	7.50	2.87	7.28	46.4	6.8	7.9
44	18.5	−0.7	1.83	0	N	P	1127.8	1116.6	0.097	2.07	7.78	229.1	2.57	0.84	9.22	0.18	0.42	1.5	1.2	1.0
45	18.5	1.5	5.65	0	N	R	1127.8	1116.2	0.100	2.07	7.05	232.8	6.04	1.17	9.71	0.04	0.10	0.5	0.7	0.7
46	18.5	1.5	5.65	0	Y	P	1127.8	1116.2	0.100	2.07	7.05	232.8	6.04	1.17	9.71	0.04	0.10	0.5	0.7	0.7
47	19.5	7.7	5.65	0	Y	F	1126.9	1115.0	0.103	1.94	5.17	241.8	6.19	1.30	8.73	0.55	1.33	7.2	2.7	2.7
48	19.5	12.1	5.65	0	Y	N	1126.9	1114.1	0.111	1.94	4.18	286.8	6.30	1.63	7.97	1.66	4.76	27.1	5.2	5.2
49	18.5	−0.7	2.26	0	Y	P	1127.8	1116.6	0.097	2.07	7.78	229.1	3.01	0.89	9.74	0.04	0.09	0.3	0.6	0.5
50	18.5	1.2	2.26	0	Y	P	1127.8	1116.3	0.100	2.07	7.16	232.5	3.03	0.92	9.71	0.04	0.10	0.4	0.6	0.5

51	18.5	4.2	3.64	0	N	L	1127.8	1003.2	1.081	2.07	6.15	295.5	7.87	7.89	9.65	0.05	0.14	3.9	2.0	1.0
52	18.6	3.0	3.64	3.5	N	P	1127.7	1115.9	0.102	2.06	6.55	234.8	4.37	1.07	9.62	0.06	0.13	0.6	0.8	0.7
53	19.5	6.3	3.64	3.5	N	R	1126.9	1115.2	0.101	1.94	5.54	234.7	4.43	1.11	8.86	0.42	0.99	4.7	2.2	2.0
54	19.5	11.5	3.64	3.5	N	F	1126.9	1114.2	0.110	1.94	4.29	277.0	4.52	1.40	8.13	1.35	3.74	18.9	4.3	3.9
55	19.5	13.2	3.64	3.5	N	L	1126.9	1113.9	0.113	1.94	3.97	308.8	4.55	1.59	7.62	2.52	7.78	40.2	6.3	5.6
56	19.5	11.6	7.37	3.5	N	L	1126.9	1114.2	0.110	1.94	4.27	278.6	7.67	1.68	8.10	1.40	3.90	23.6	4.9	5.2
57	19.5	6.9	7.37	3.5	N	F	1126.9	1115.1	0.102	1.94	5.38	237.6	7.53	1.35	8.81	0.46	1.09	6.2	2.5	2.7
58	19.4	6.5	7.37	3.5	N	R	1127.0	1115.2	0.102	1.95	5.49	236.9	7.51	1.34	8.91	0.38	0.90	5.1	2.3	2.5
59	19.4	8.8	7.37	6.5	Y	R	1127.0	1114.7	0.106	1.95	4.89	250.2	7.59	1.46	8.68	0.59	1.48	8.6	2.9	3.2
60	19.5	11.4	6.95	6.5	Y	F	1126.9	1114.2	0.110	1.94	4.31	275.5	7.34	1.64	8.15	1.32	3.64	21.6	4.6	4.9
61	18.5	12.1	6.95	6.5	Y	L	1127.8	1114.1	0.119	2.07	4.18	316.4	7.36	1.90	9.22	0.18	0.57	3.4	1.8	1.9
62	18.5	7.5	6.95	6.5	Y	F	1127.8	1115.0	0.111	2.07	5.23	255.0	7.23	1.45	9.55	0.07	0.17	1.0	1.0	1.0
63	18.5	3.5	6.95	6.5	Y	P	1127.8	1115.8	0.104	2.07	6.38	237.0	7.12	1.28	9.67	0.05	0.11	0.6	0.8	0.8
64	20.0	3.8	3.47	1.5	N	P	1126.4	1115.7	0.093	1.87	6.28	222.2	4.21	1.00	8.77	0.50	1.11	5.0	2.2	2.1
65	20.0	9.8	3.47	0	N	F	1126.4	1114.5	0.103	1.87	4.63	247.3	4.33	1.21	8.04	1.52	3.76	18.4	4.3	3.8
66	20.0	12.1	3.47	0	N	L	1126.4	1114.1	0.107	1.87	4.18	274.3	4.37	1.38	7.47	2.97	8.15	41.0	6.4	5.7
67	20.0	10.5	3.47	0	N	F	1126.4	1114.4	0.104	1.87	4.48	253.9	4.34	1.25	7.89	1.84	4.67	23.0	4.8	4.3
68	20.0	2.5	3.47	0	N	R	1126.4	1116.0	0.090	1.87	6.72	220.6	4.19	0.98	8.86	0.42	0.93	4.1	2.0	1.9
69	20.0	2.0	3.47	0	N	R	1126.4	1116.1	0.089	1.87	6.89	158.3	4.18	0.97	8.89	0.39	0.59	3.3	1.8	1.5
70	19.2	11.6	3.47	6.5	Y	—	1127.1	1114.2	0.112	1.98	4.27	286.0	—	—	8.42	0.90	2.57	—	—	—
71	19.3	11.6	3.32	6.5	Y	F	1127.1	1114.2	0.112	1.97	4.27	283.3	4.22	1.40	8.31	1.06	3.00	14.8	3.9	3.4
72	19.1	4.0	3.32	6.5	Y	P	1127.2	1115.7	0.100	1.99	6.21	231.6	4.09	1.04	9.27	0.17	0.40	1.8	1.3	1.2

TABLE 1. Conditions and dimensionless variables for constant-flow-rate experiments, Nos. 25–72. All variables defined in text. All units are in m.k.s. except r_s which is in c.g.s. 'Type' refers to dominant morphology: N = no crust, L = levees, F = folding, R = rifting, P = pillows. Slope of tank is listed in degrees. Subscript a refers to ambient field (sucrose solution). No subscript or '1' refers to PEG. Θ_s for experiments nos. 36–45 are based on T_s of 17 °C for that particular batch of wax. For all other runs, T_s is assumed to be 18 °C.

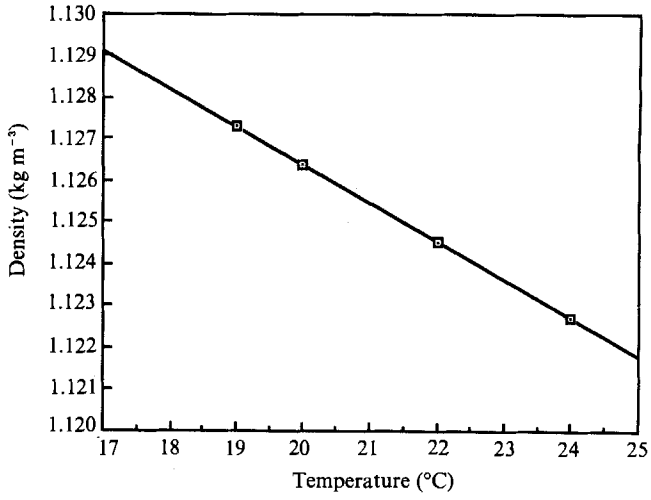

FIGURE 4. Plot of density versus temperature for clear PEG 600.

time interval were averaged, and plots of radius versus time were generated. Average flow-front velocities and horizontal strain rates were also computed from the radius versus time plots. Side views were digitized to allow measurement of topographic profiles through the flows.

Experiments nos. 1–24 used a gravity feed (in place of constant flow rate) of a fixed quantity of wax from a suspended reservoir into the base of the tank through a 1.1 m long hose. Actual volume flow rates decreased steadily during the course of each experiment. Mean flow rates were calculated from the time taken to release a known volume. The total amount of wax varied somewhat from one run to the next because in some cases the experiment was stopped before the reservoir had completely drained. The sequence of experiments allowed us to investigate behavioural changes that accompanied a decrease in the volume flow rate.

The final 18 experiments (table 1) used a larger (60 cm diameter) circular tank which had two available inlet holes, one in the centre and one 10 cm from the edge. The tank also had a target visible beneath the base which had inscribed circles spaced 2 cm apart. The larger radius permitted experiments to be run for longer times. Tilting of the tank allowed observation of the effect of underlying slope on flow dynamics and morphology.

An additional parameter that could be varied was the roughness of the bottom of the tank. In several of the constant-flow-rate runs using both square and circular tanks, a brass screen with 0.3 mm square mesh was placed on the smooth surface to increase basal friction.

The solid wax was stored in covered 20 l plastic containers. Before being used, these were heated to approximately 35 °C to melt any fragments of solid wax and then were allowed to cool to the experimental temperature. Each container could supply 5–10 experiments. Densities of the wax (ρ_l) and the sucrose solution (ρ_a) were measured with an Anton Paar DMA 60 density meter, to an accuracy of $\pm 0.002\%$. The kinematic viscosity (ν) of each new batch of wax was measured as a fraction of temperature using a Cannon–Fenske capillary viscometer. We estimate that some of these viscosity readings may have only been accurate to within 5%. Plots of density and viscosity versus temperature for a representative batch of PEG 600 are shown in Figures 4 and 5.

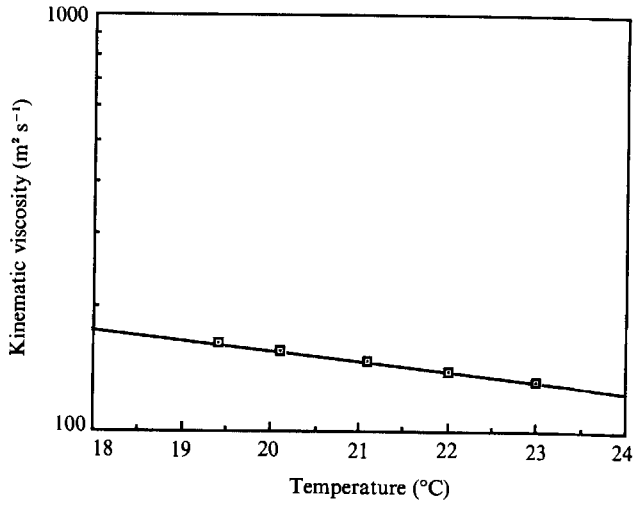

FIGURE 5. Plot of kinematic viscosity versus temperature for a representative batch of clear PEG 600. As the temperature approaches T_s, the viscosity increases much more rapidly.

There are two drawbacks to using PEG 600. First, at relatively high temperatures ($\geqslant 15$ °C) or after long times ($\geqslant 10$ minutes), mass diffusion of wax into water can become significant, which effectively decreases the observed spreading rate and the temperature contrast between wax and surroundings. Second, rather than having a precise freezing point, solidification of the wax can take place over a range of temperatures (17–20 °C), depending on the exact molecular make-up of a particular batch. This makes it difficult to define a consistent solidification temperature for scaling calculations. Furthermore, if wax in the reservoir is kept within its solidification range for an extended period of time (more than about two weeks), it can become a cloudy suspension with a significantly higher viscosity. In a few experiments we intentionally allowed this condition to develop, but in general we monitored the appearance of the wax in the reservoir to maintain it in a clear state with no solid fragments. Use of only one fluid does, of course, limit our experiments to only one value of the solid yield strength σ_y, hence a very limited range of values for the strength parameter Σ.

4. Spreading rates

One of the principal motivations for this study was to improve the interpretation of dynamic and morphologic data obtained from lava flows and domes. In their field investigation of an actively growing lava dome, Huppert *et al.* (1982) used the theoretically predicted and experimentally confirmed relationship (1) between radius and time to estimate the bulk viscosity of the flow. They calculated a much larger value than those obtained in the laboratory, and attributed the different result to the presence of solid blocks and a cooled surface crust, neither of which was directly accounted for by their theory or experiments. Other field studies of lava flows (e.g. Pinkerton & Sparks 1978; Fink & Zimbelman 1986) similarly give much higher viscosity values than laboratory determinations.

The first goal of our experiments was to quantify the influence of surface crust on the radial spreading of viscous–gravity currents. To this end, we compared our data for flow-front position versus time for constant-effusion-rate experiments with those

obtained by Huppert (1982) for the spreading of very viscous oils in air. For his isothermal experiments, Huppert found excellent agreement with

$$r^* = \frac{r}{(0.715)(g'Q^3/3\nu)^{\frac{1}{8}}} = t^{\frac{1}{2}}. \tag{14}$$

We expected to find a similar time-dependence of radius for those of our experiments in which the influence of solidification was negligible. For experiments in which cooled surface crusts were observed, we anticipated deviations from the square-root time-dependence.

Figure 6 is a representative plot of dimensionless radius versus time for one of our experiments (no. 35) in which crust did not appear. To first order, the results are close to those found in isothermal experiments. However, closer examination reveals that the radii are systematically less than the values indicated by (14), and may be better represented by

$$r^* = \frac{r}{(0.715)(g'Q^3/3\nu)^{\frac{1}{8}}} = t^{0.45}, \tag{15}$$

in which ν is taken as the viscosity measured at the extrusion temperature of the wax. The slight discrepancy in time-dependence between (14) and (15) can be explained by assuming that the upper and lower portions of the wax flow cooled and became more viscous, even though they did not solidify.

Figure 7 shows the results for four experiments with increasing cooling rates indicated by systematically lower values of t_s, the time necessary for crust to first appear. Huppert's isothermal result (14) is also shown. The effect of cooling on the spreading rate is clearly seen: the colder the experiment, the smaller the radius for a given time. In addition, at relatively large times the trends of the spreading rate plots show distinct kinks. Spreading after these transition points is appreciably slowed, a behaviour that could be caused by the appearance of an effective yield strength (σ_y) associated with development of the solid crust.

Some support for the role of a developing yield strength is provided by our observations of the distribution and thickness of crust. For relatively mild cooling rates the surface crust was slow to form and significant thickening occurred only at the nose of the spreading front, constructing a levee bank. Crust that formed on the mobile surface behind the front was advected toward the front and added to the levee construction. As a levee grew, the flow upstream slowed and became deeper, until the levee broke and was pushed aside by escaping liquid. We could see nothing regular or axisymmetric in the formation and breaking of levees. Only occasionally did liquid wax spill out over the top of an unbroken levee. Under conditions giving rise to levees the transition in spreading rate was associated with a greatly reduced frequency of breakthrough and a greater tendency for crust to extend upstream from the levee. For rapid cooling rates solid crust developed almost everywhere over the wax surface. The area free of crust decreased in time as velocities decreased in response to both radial spreading and decreasing flow depth. These crust-free areas were limited to the axes of rifts (lines of separation of large rigid plates of crust and of flow divergence) or to occasional narrow crevices through which liquid temporarily escaped to produce new lobate structures. The transition in spreading rate appeared to occur when velocities decreased and rift lines froze over. Further spreading required new lines of weakness to open.

The simplest flow system that incorporates a yield strength is the spreading of a Bingham plastic (Blake 1990). In that case the flow is characterized by a transition

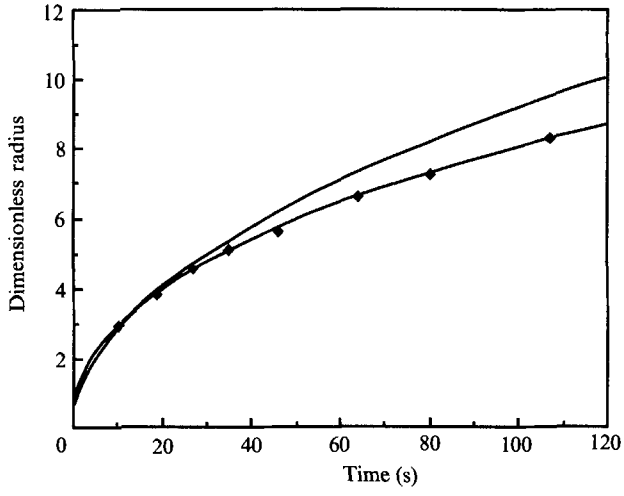

FIGURE 6. Plot of dimensionless radius versus time for experiment no. 35 ($Pe = 543$, $\Theta_s = 0.56$), in which no visible crust formed. Also shown is the line predicted by theory (Huppert 1982) for spread of an isothermal Newtonian fluid.

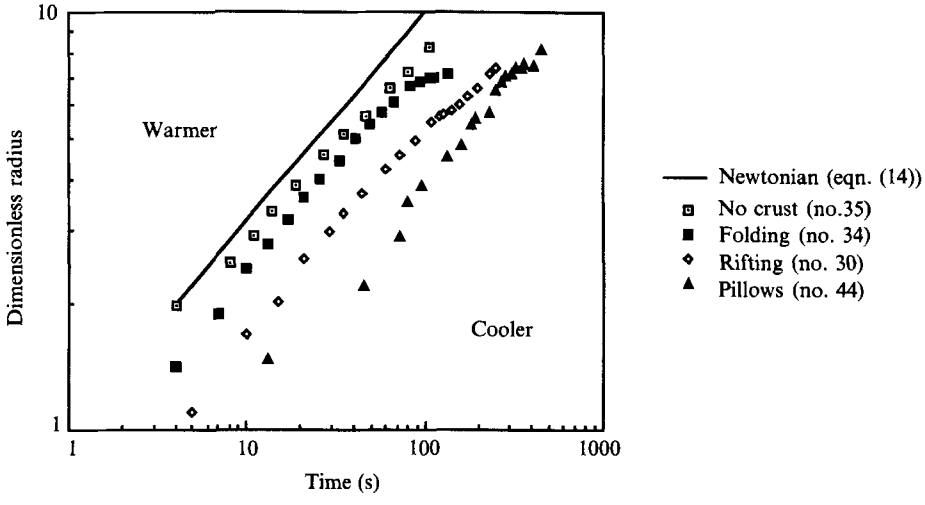

FIGURE 7. Plot of dimensionless radius versus time for four experiments showing the decreased spreading rate and changes in morphology accompanying decreases in dimensionless temperature. The folding and rifting runs exhibit distinct decreases in slope at large values of time. Radii plotted are the averages of measurements at eight points 45° apart and have standard errors ranging from 3% for no-crust conditions to nearly 28% for pillow conditions. The large scatter in the pillow data reflects the irregular bud-like growth pattern of the flow.

from Newtonian viscous spreading during an initial phase to Bingham behaviour in which buoyancy and (a constant) yield strength are dominant. Analogous behaviour is likely to occur in the solidifying flow, and this is the reason why a number of investigators have modelled lava flows as Bingham plastics. The yield strength, however, is found only in the solidified portion of the flow, a portion that is developing in thickness and connectivity as the spreading proceeds. Hence the effective yield strength must increase in time under all conditions other than those in which internal 'lava tubes' supply liquid directly to the front.

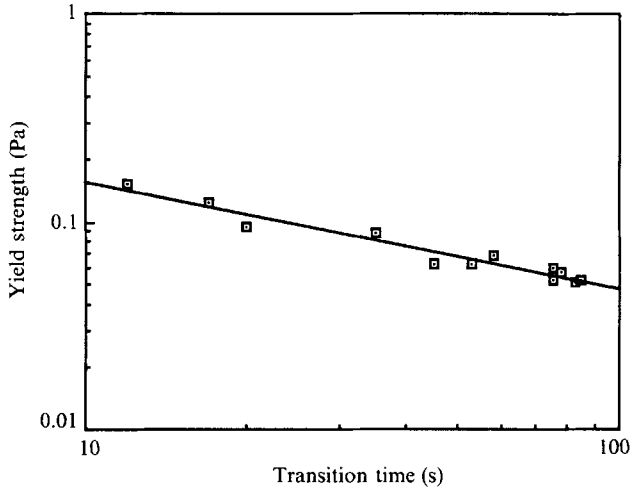

FIGURE 8. Plot of yield strength versus transition time based on equation (17), after Blake (1990). Transition times were determined from changes in slope identified in radius-versus-time plots.

A Bingham material with a yield strength has a minimum thickness (h_0) below which it is not able to flow:

$$h_0 = \frac{\sigma_y}{\rho g \sin\beta}. \tag{16}$$

Thus, if we compare two axisymmetric flows, identical except that only one has a yield strength, the Bingham flow will be thicker at the margins and will have spread less far than the Newtonian one at a given time. Blake (1990) found that a transition from Newtonian to Bingham behaviour occurred after a time, t_B, defined as

$$t_B = \left(\frac{\rho^8 g'^3 \nu^5 Q}{\sigma_y^8}\right)^{0.25}. \tag{17}$$

If we assume that the kinks in our radial-spreading plots correspond to the onset of Bingham behaviour, we can use the observed transition times to calculate the yield strengths. For those of our experiments in which crusts formed, transition times to calculate the yield strengths. For those of our experiments in which crusts formed, transition times ranged from 12–88 s. Combining these times with measured physical properties, we used (17) to estimate the 'effective' yield strength of the wax at the time Newtonian spreading, as defined by (14), ceased. These strength values are shown in figure 8. We can compare these estimated yield strengths with values based on the observed thicknesses of the flows. For a typical experiment (no. 33) with slow crust formation ($t_B = 78$ s), (17) predicts a strength of 0.06 Pa. Using (16), this strength corresponds to a minimum thickness of 0.5 mm, similar to a value of 0.3 mm estimated from side photographs. For another experiment (no. 41) in which crust formation was more rapid ($t_B = 35$ s), (16) suggests a minimum thickness of 0.7 mm, again consistent with an estimated value of 0.8 mm.

5. Surface morphology

Several types of surface morphology have been used by geologists to determine the conditions under which lava flows form. Such studies typically begin with the identification of relatively simple structures in the complex surfaces of natural flows. Theoretical models are then used to relate the geometry of these features to the

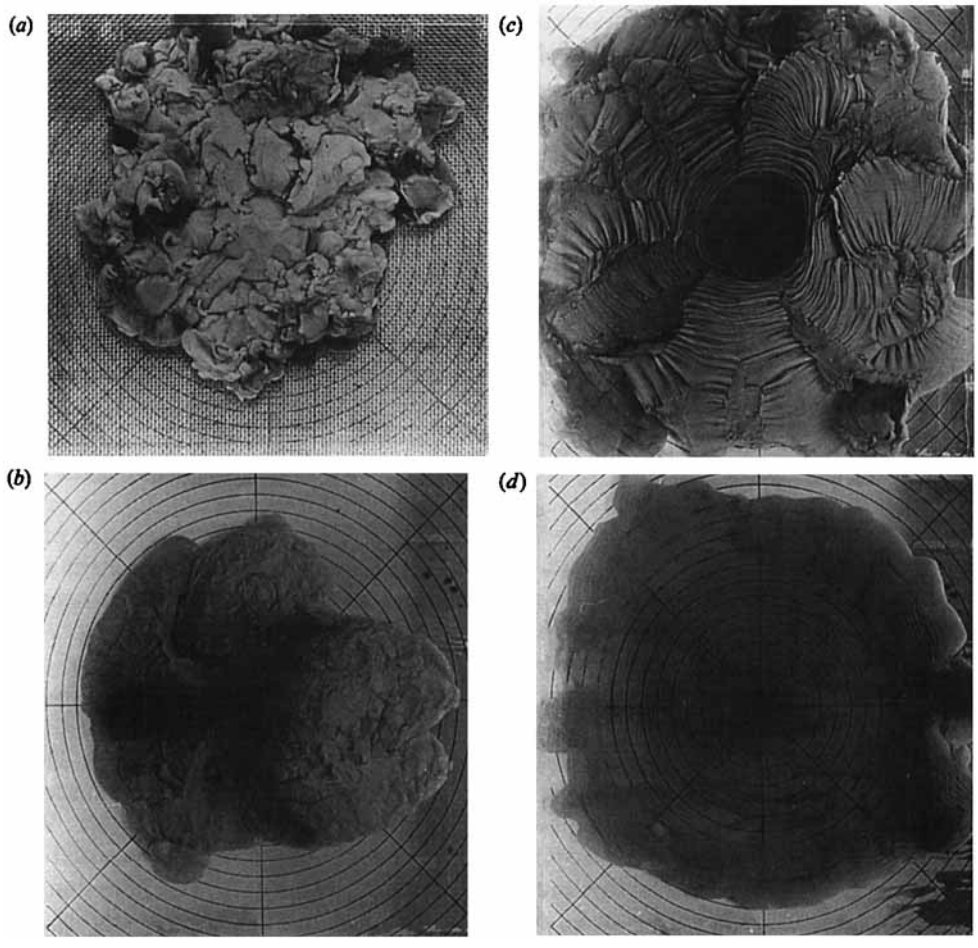

FIGURE 9. Plan-view photographs of experiments with a horizontal base: (*a*) no. 46 ($t = 162$ s) showing 'pillow' growth; (*b*) no. 30 ($t = 190$ s) showing development of a three-armed rift structure; (*c*) no. 32 ($t = 162$ s) showing formation of folds; and (*d*) no. 36 ($t = 300$ s) showing levee formation. Basal mesh is present in (*a*) only. Field of view is 30 cm across. For experiment parameters, see table 1.

rheology, local state of stress, and temperature distribution thought to have been present in the active lava. This part of the exercise is the least exact, as it is always difficult (and often impossible) to measure rheological and thermal properties of active lavas. Laboratory simulations potentially allow more accurate specification of both the geometric and rheological requirements for the formation of particular structures.

Our experiments generated a remarkably reproducible sequence of morphologies (figure 9). These also resembled those found in lava flows. The crustal morphology depended on the relative rates of crust formation and radial spreading. We report first the results for a horizontal base and later indicate some of the effects of bottom slope.

In experiments with the slowest extrusion rates (lowest Pe or Π values) or lowest bath temperatures (highest Θ_s or lowest τ_s), cooling is most efficient and crust forms almost immediately as the wax emerges. This solid wax forms a connected shell which prevents the liquid interior of the current from advancing. Confinement raises

the internal pressure in the dome or tube, stretching or bending the crust until its tensile strength is exceeded. At this point a break-out occurs. After a small volume of wax has escaped, its newly exposed surface again solidifies rapidly. This episodic process of advance, freezing, and pressure build-up results in a collection of interconnected bulbous lobes, or pillows (figure 9*a*). The dimensions of the lobes were clearly smaller for larger temperature contrasts (Θ_s closer to one). The extrusion builds up a dome which can be as high as it is wide. When dissected, the dome is found to consist of a large number of interconnected cavities of liquid wax.

For slightly higher extrusion rates (or lower cooling rates), crust first appears at some distance from the centre and then propagates back toward the vent, but without ever forming a fully connected shell. Instead, local tension over the vent pulls the crust apart at roughly the same rate that it forms. The result is a structure with three or four wedge-shaped solid plates maintained (at least for a time) at a constant distance from each other (figure 9*b*). The hotter interior wax continues to fill the radial gaps or *rifts* between the solid plates. Associated with the divergent flow within these zones are circumferential striations in the thin, newly solidifying crust. There are also regular patterns of step-like offsets in the axes of the rifts, each offset being the focus of a line on the wax surface which runs perpendicular to each rift axis. These features have a very similar appearance to the transform faults in oceanic crust along mid-ocean spreading centres.

In runs with still higher extrusion rates (or lower cooling rates), solidification only occurs in narrow zones forming radial strips of crust. Because of the outward decrease in radial velocity, these strips experience radial compression. If this compression is strong enough, it can result in surface folding (figure 9*c*). This is the type of buckling that can occur when a stronger (or more viscous) layer of material bounded by a less viscous fluid is acted upon by a compressive load (Biot 1961; Fink & Fletcher 1978). In this case the longer the strips, the greater the stress imposed and the more likely a crust of given thickness is to buckle. Eventually the folded strips may merge to form a continuous set of circular folds surrounding the vent (figure 9*c*). The liquid surface between the strips at larger radii may also freeze over, partially welding the folded strips together.

For experiments with the highest extrusion (or lowest cooling rates), crust only appears in the most distal portion of the current. As a result, it does not experience a sufficiently large underlying velocity difference to cause folding. At a distance where the radial velocity of the front becomes small enough, the solid crust may be able to form a complete ring (figure 9*d*), confining the liquid portion of the flow until it spills over or breaks through this circumferential structure, which we refer to as a levee. In some runs, thin crust close behind the levee eventually began to fold at large times. This behaviour does not blur the distinction between the two types of flow structure but does introduce a small uncertainty into the position of the transition in parameter space.

In theory, whenever wax is injected into a bath that is colder than the wax freezing point i.e. $T_a < T_s$ solid crust should develop. In practice, the finite size of our tank meant that in those experiments with the highest extrusion rates (and lowest cooling rates) the flows reached the boundaries before cooling sufficiently to form any crust. We designate these flows as having had no crust, although this does not imply that crust would not have developed if the width of the tank had been much greater and molecular diffusion of wax and water were absent.

In some experiments more than one type of structure was observed; however, usually only one was dominant. The folding instability, as mentioned above,

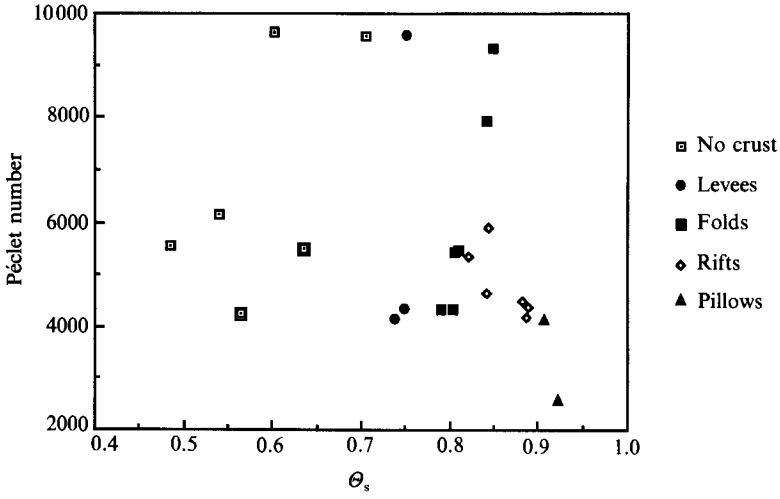

FIGURE 10. Plot showing type of dominant structure seen at various value of Pe and Θ_s, for 23 constant-effusion-rate runs with clear wax, in the flat tank, with no basal mesh.

sometimes did not occur until late in the experiment, with much of the spreading involving only frontal levees. In these transitional cases 'levees' were classed the dominant structure. Similarly, some conditions intermediate between those giving 'folds' and those giving only 'rifts' between rigid plates gave a combination of folding and rifting processes, with solid plates tending to become more rigid as the flow spread. Folding and rifting do occur simultaneously in many other runs: folds form in response to radial compressive stress; rifts in response to simultaneous circumferential tension and flow divergence created by radial spreading. Hence conditions classed as 'folding' generally imply a type of rifting as well. In contrast, conditions classed as 'rifting' do not give rise to folds and the rifts themselves tend to take on a different appearance: they have fewer 'arms' (between 1 and 5) radiating from the vent during the early stages of spreading, and commonly contain the perpendicular striations and staircase offsets described earlier. Thus each run could be classed unambiguously as dominated by either 'pillows', 'rifting', 'folding', 'levees', or as having 'no crust'.

Figure 10 summarizes the dominant morphology for 23 runs with constant effusion rates onto a horizontal floor without basal mesh. The dominant type of surface structure is clearly related to the flow rate and temperature conditions as described by Pe and Θ_s. The principal types occur in fairly well-defined zones of this parameter space. For a given set of wax and ambient temperatures (i.e. constant Θ_s), structures associated with rapid crust formation (pillows, rifts) are favoured by decreasing values of Pe. Similarly, for constant Pe, crust formation is promoted by increasing Θ_s.

All experiments utilized the same wax and a limited range of sugar concentrations in the overlying water. Hence each run has approximately the same values for the strengths of the solidified wax (up to an unknown temperature dependence) and for the physical properties of the water. This greatly limits the possibility for extrapolation of the results to other systems such as natural lava flows. One step in this direction, however, is to replace Pe by the modified Péclet number Π, thus including the parameters affecting the turbulent convective heat flux from the wax surface. Figure 11 shows the data of figure 10 expressed in terms of Π. In order to

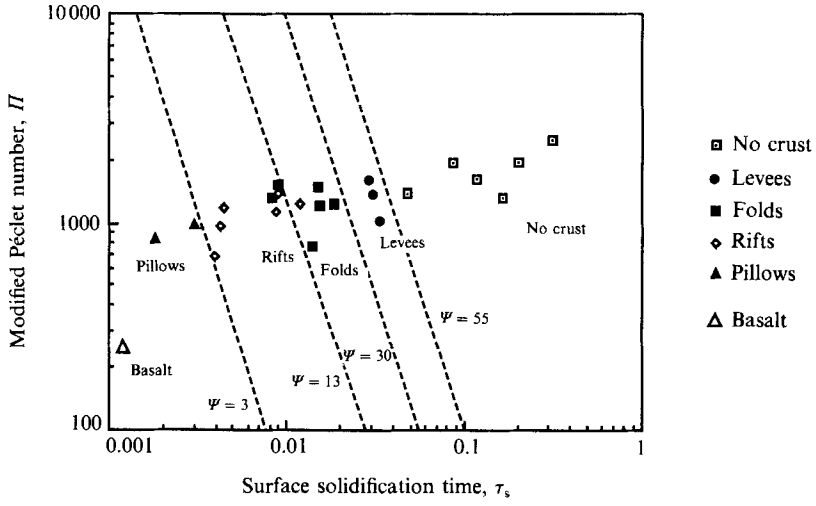

FIGURE 11. Plot showing the same information as figure 10, but expressed in terms of the modified Péclet number (Π) and the dimensionless time to solidification (τ_s). Lines representing constant Ψ separate the different morphologic fields. Calculated values of Π and τ_s for the submarine pillow data are shown for comparison.

assist physical interpretation of the results, Θ_s is also converted into the corresponding dimensionless time τ_s required for solidification to begin (t_s normalized by the timescale for surface cooling, λ). Again the major crustal structures occur in well-defined zones, and the transitions can now be related to specific values of the single dimensionless variable Ψ given by (10). For example, transition from no crust to levees is found to correspond to the value $\Psi \approx 55$. This dependence of morphology on Ψ is consistent with our hypothesis that the behaviour is determined by the rate of formation of crust. However, the limited range of values achieved for Π, and an even more limited range of Σ values, precludes a full test.

From the results on figure 11 and relation (13) it is possible to estimate the distance from the vent to the point of surface solidification. At $\Psi = 55$, solidification is predicted to begin at $r_s/H = 7.4$, or $r_s \approx 9$ cm (since (1) gives $H \approx 1.2$ cm). Similarly, folding, rifting and pillow formation require solidification to begin less than 6 cm, 3.6 cm and 1.7 cm, respectively, from the vent. These values appear to be consistent with those at which solid crust could be seen in the experiments, although the distance could not be determined to better than 1–2 cm. Solidification also occurred closer to the vent as each extrusion developed in time. This was often due to formation of internal pathways (through tubes or chambers) by which the liquid wax reached the surface distant from the vent.

The full effects of a bottom slope on the spreading of viscous flows are beyond the scope of this paper. However, the influence of a small slope on the types of crustal deformation is easily seen and it is useful to compare the results with those for a horizontal base. We conducted experiments on a 6.5° slope over a similar range of conditions. Under conditions that would be expected to give pillow-like development of the wax dome we found that the bottom slope had little effect. The dome initially grew by irregular budding and freezing over, spreading irrespective of the direction of the slope. After the radius of the dome covered a basal elevation difference comparable with the height of the dome (also comparable with the radius), there was a weak tendency for greater downslope spreading, again by pillow formation. Conditions that give rifting behaviour on the slope are unchanged from those on

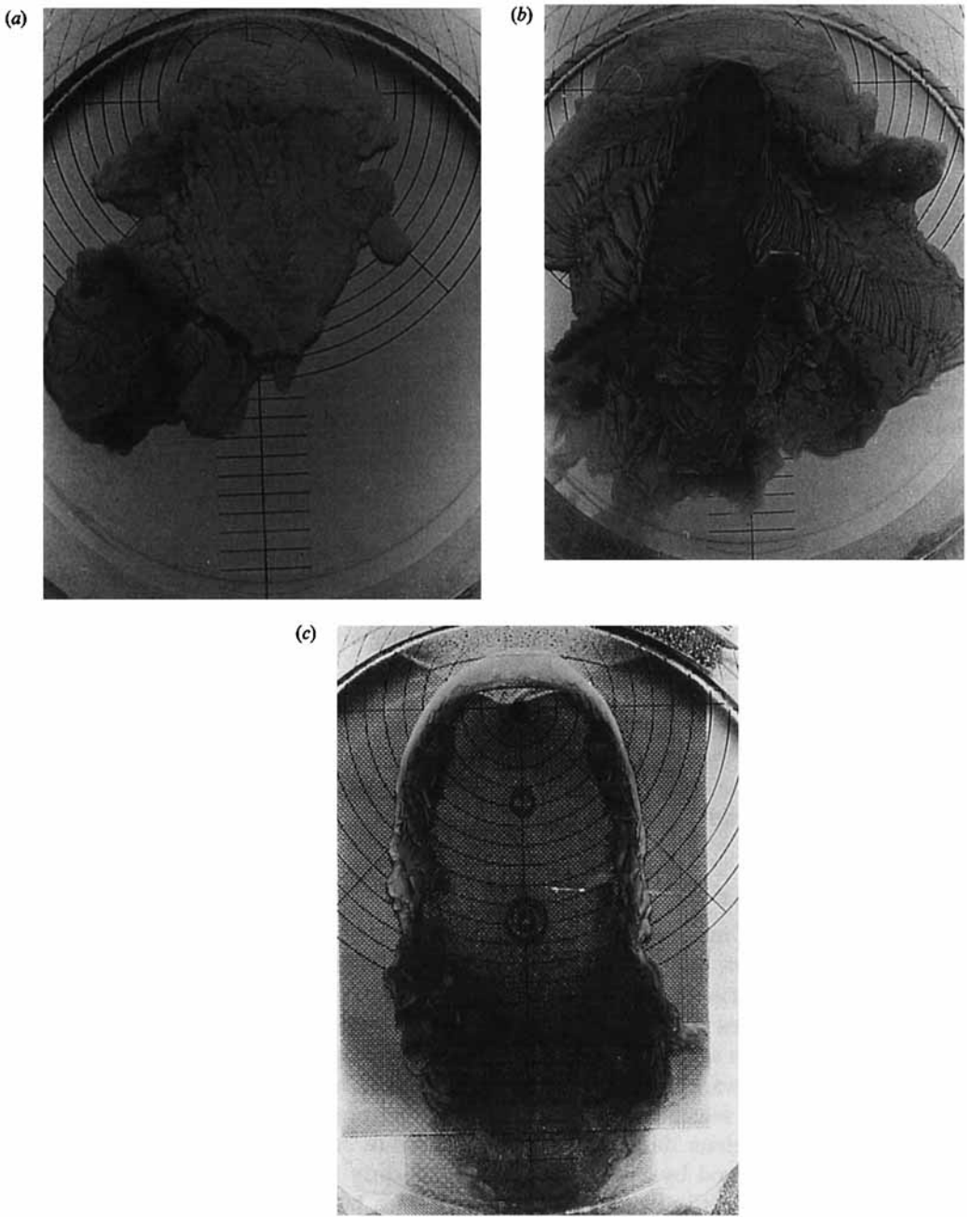

FIGURE 12. Photographs of experiments with a sloping base: (*a*) no. 58 ($\beta = 3.0°, t = 305$ s) showing 'rifting' (the first rift has ceased near source at top and a second rift is now active); (*b*) no. 57 ($\beta = 3.0°$, $t = 452$ s) showing folding; (*c*) no. 60 ($\beta = 6.5°$, $t = 263$ s) showing formation of levees around the margins of the flow. Tank is 60 cm in diameter. Wire mesh covers the floor in (*c*). For experiment parameters, see table 1.

figure 11. On the slope, however, there is a tendency for an initial single rift to develop with its axis aligned across the slope, its ends sometimes curving downslope (figure 12*a*). Thereafter the spreading is predominantly in the downslope direction.

Similarly the slope did not alter conditions giving rise to folding or levees. The flows simply became asymmetric, with folds (figure 12*b*) or levees (12*c*) occurring sooner on the upslope side than on the downslope and rapidly forming a rigid, stationary crust on the upslope side. The wax proceeded to spread downslope in an active channel with compressive stresses on the crust being confined largely to the sides and downslope front of the channel. Crust developed most rapidly where flow velocities were smallest. We speculate that greater slopes would, by increasing flow velocities downslope, probably favour the formation of levees over the development of larger regions of folded crust, or rifting over pillow growth.

The basal mesh had roughly the opposite effect of a bottom slope. It provided some resistance to both lateral and downslope spreading of the flows. Thus in experiments whose Ψ values suggested levee formation with no folding, the mesh led to folding. However, the influence of the added basal friction tended to increase compressive stresses at the expense of tension. Thus central rifts, which require large tensile stresses over the vent, were not observed in any experiments conducted with the basal mesh, although radial fractures were seen near the outer portions of several of these flows. The advance of new lobes of escaping liquid at large cooling rates may also have been slowed, assisting formation of pillows in place of rifts. Thus the overall effect of the mesh may have been to expand the folding and pillow fields in figure 12 and to reduce the rifting region.

Finally, each of the fixed-volume experiments (nos. 1–24) showed similar behaviour to that found in one or more of the constant-extrusion-rate runs. Again, in most cases, only one morphologic type was observed despite a decrease of the inflow rate with time. This might be because the total emplacement times and volumes were too small to allow more than a single deformation regime to occur.

6. Application to lava flows

The main purpose of our experiments was to provide insight into the dynamics of lava flow emplacement, particularly the effects of surface solidification on flow dynamics and deformation of the solid crust. The general conclusion that a range of common flow structures can be generated by varying either the flow rate or the ambient temperature is a useful qualitative tool for interpreting lavas. Where data exist for active lava flows, comparison of their behaviour with that of the laboratory wax extrusions shows reasonable agreement. For example, documentation of the growing Mount St. Helens dacite dome shows that in several extrusive episodes, early folding was followed by late rifting, corresponding to a decrease in extrusion rate and Péclet number. Similarly, in many Hawaiian pahoehoe basalt flows, late-stage pillow-like forms (referred to as 'toey pahoehoe') develop after extensive branching lowers the local volume flow rate. In the 1984 Mauna Loa aa flow, levee formation in the middle reaches was followed by late-stage folding as the flow rate was reduced.

In order to better assess the relevance of the wax experiments and cooling analysis to natural flows, we here attempt a quantitative comparison. Because our experiments match conductive heat loss in the wax to convection in the ambient fluid, we focus on a natural situation in which similar heat loss mechanisms take place. We consider the conditions necessary for a 1 m thick submarine basalt flow to

develop pillow structures. Figure 11 indicates that pillow formation requires $\Psi \leqslant 3$. From (13) this implies that $r_s/H \leqslant 1.7$. In other words, if the interior of the flow is exposed along a fresh spreading crack, it should cool to the solidification temperature on travelling a distance less than 1.7 m. Tepley & Moore (1974) filmed pillows forming on active submarine basalt flows. They showed that lava emerging from glowing cracks cools from red to black within approximately 20 cm. The formation of pillows is therefore consistent with the above predictions based on our experiments.

Tepley & Moore's (1974) film allows a further check of the applicability of our laboratory results. The cooling they showed occurred in growing tube-shapes pillows which have diameters of about 0.4 m. The lava that emerged from the cracks had a velocity of about 0.1 m s^{-1}, giving a local volume flow rate of $Q = 0.03$ m^3 s^{-1}. If we take measured lava and water properties†, we can calculate from (8*b*) that $\lambda = 13.9$ s, from (3) that $Pe = 4.9 \times 10^5$, and from (10) that $\Pi = 2.5 \times 10^2$. The temperatures also indicate that $\Theta_s \approx 0.96$, from which we compute $\tau_s \sim 10^{-3}$. Referring again to figure 11, we see that the point defined by $\Pi = 2 \times 10^2$ and $\tau_s = 10^{-3}$ lies well within the field of pillows. Even if a much greater volume flux was used in place of the very local value above, the weak dependence of Π on Q suggests that this flow would still lie in the pillow regime. This comparison, though apparently successful, should be viewed with caution since we have taken no account of any difference in the relative magnitudes of crustal strength and buoyancy.

In contrast to submarine basalts and our experimental flows, sub-aerial lavas lose most of their heat by radiation into the air. In order to apply our experimental results to such a configuration, we would need to incorporate a slightly different thermal boundary condition. Such an analysis would give a different formulation for the timescale λ and for the modified Péclet number, Π. Otherwise, the dimensionless results shown in figure 12 should continue to apply, since the flow morphology is again likely to be controlled primarily by the relative rates of crustal thickening and lateral spreading.

Although we did not include the effect of the basal mesh in our dimensional analyses, the mesh thickness was about 1 mm, compared to a typical flow depth of about 8 mm. Thus the ratio of basal roughness to flow thickness was about 1:8. Natural lava flows passing through forested or developed areas would be likely to encounter obstructions of this scale, while those flowing over earlier-emplaced lavas or more open terrain would face conditions more analogous to those in the smooth-floored tank. Furthermore, the advance of most silicic and aa-type basalt flows is retarded by the presence of a thick snout of blocky lava. This resistance may be qualitatively simulated in experiments by the presence of a basal mesh.

Despite the various unexplored factors, the general agreement between our experimental results and the above calculations suggests that our cooling analysis accounts for the major processes controlling the morphology of lava flows. Before this study can be used with confidence for more general interpretation of lava flows, additional field measurements like those presented by Tepley & Moore (1974) will be needed to allow better specification of the domains in which different structures form. Once such regions are defined, then the distribution of surface morphology on prehistoric or remotely observed flows may be used to better constrain flow conditions.

† Turcotte & Schubert (1982) give the following properties for basaltic lava: $T_l = 1150$ °C, $T_s = 1100$ °C, $c = 1.2 \times 10^3$ J kg^{-1} K^{-1}, $\rho = 2.8 \times 10^3$ kg m^{-3}, $\kappa = 5 \times 10^{-7}$ m^2 s^{-1}, $\nu = 4 \times 10^{-2}$ m^2 s^{-1}. Water properties are $T_a = 0$ °C, $c_a = 4 \times 10^3$ J kg^{-1} K^{-1}, $\rho_a = 1.0 \times 10^3$ kg m^{-3}, $\kappa_a = 1.4 \times 10^{-7}$ m^2 s^{-1}, and $\nu_a = 10^{-6}$ m^2 s^{-1}.

7. Summary

We have used laboratory experiments to show that the morphology and dynamics of viscous–gravity currents with solidifying crusts are largely controlled by a balance between extrusion rate and the rate of formation of solid crust. As parameters were varied, a sequence of distinct and unambiguously recognizable structural features were formed by the solidifying crust. For a given flow rate, progressively increasing the temperature contrast leads to the production of marginal levees, surface folds, rift-like centres of spreading, or bulbous pillows. Decreasing the extrusion rate for a set temperature contrast yields the same sequence of structures. Theoretical analysis of the experimental cooling conditions showed that a Péclet number Pe and a temperature parameter Θ_s could be combined into a single dimensionless number, Ψ, which describes the time needed to freeze the flow surface. Regimes giving different surface morphology are then separated by values of this single variable. A possible additional influence of the magnitude of the strength of the solid crust could not be investigated. Along with the changing nature of surface deformations there was a strong and consistent variation of the influence of the solidified crust on the overall rate of spreading of the flow.

Successful application of these results to natural lava flows will require calibration through detailed field observations and measurement of material properties. Initial comparison with the relatively well-documented formation of submarine pillow basalts shows some quantitative agreement with both our theoretical and experimental results.

The authors thank Derek Corrigan, Tony Beasley and Ross Wylde-Browne for assistance in setting up and running the laboratory experiments, and Stewart Turner, John Lister and Herbert Huppert for helpful discussions. Steven Baloga and an anonymous referee provided constructive reviews. J.H.F. was supported by NASA grant NAGW 529 from the Planetary Geology and Geophysics Program, and a visiting fellowship from the Research School of Earth Sciences at The Australian National University.

REFERENCES

Anderson, S. W. & Fink, J. H. 1990 The development and distribution of lava surface textures at the Mount St. Helens dacite dome. In *Lava Flows and Domes: Emplacement Mechanisms and Hazard Implications* (ed. J. H. Fink). IAVCEI Proc. in Volcanology, vol. 2, pp. 25–46.

Baloga, S. M. 1987 Lava flows as kinematic waves. *J. Geophys. Res.* **92**, 9271–9279.

Baum, B. A., Krantz, W. B., Fink, J. H. & Dickinson, R. E. 1989 Taylor instability in rhyolite lava flows. *J. Geophys. Res.* **94**, 5815–5828.

Biot, M. A. 1961 Theory of folding of stratified viscoelastic media and its implications in tectonics and orogenesis. *Bull. Geol. Soc. Am.* **72**, 1595–1620.

Blake, S. 1990 Viscoplastic models of lava domes. In *Lava Flows and Domes: Emplacement Mechanisms and Hazard Implications* (ed. J. H. Fink). IAVCEI Proc. in Volcanology, vol. 2, pp. 88–128.

Carslaw, H. S. & Jaeger, J. C. 1959 *Conduction of Heat in Solids*. Oxford University Press.

Crisp, J. A. & Baloga, S. M. 1990 A model for lava flows with two thermal components. *J. Geophys. Res.* **95**, 1255–1270.

Didden, N. & Maxworthy, T. 1982 The viscous spreading of plane and axisymmetric gravity currents. *J. Fluid Mech.* **121**, 27–42.

Fink, J. H. 1980*a* Surface folding and viscosity of rhyolite flows. *Geology* **8**, 250–254.

FINK, J. H. 1980*b* Gravity instability in the Holocene Big and Little Glass Mountain rhyolitic obsidian flows, northern California. *Tectonophys.* **66**, 147–166.

FINK, J. H. 1983 Structure and emplacement of a rhyolitic obsidian flow: Little Glass Mountain, Medicine Lake Highland, northern California. *Bull. Geol. Soc. Am.* **94**, 362–380.

FINK, J. H. & FLETCHER, R. C. 1978 Ropy pahoehoe: Surface folding of a viscous fluid. *J. Volcanol. Geotherm. Res.* **4**, 151–170.

FINK, J. H. & ZIMBELMAN, J. R. 1986 Rheology of the 1983 Royal Gardens basalt flows, Kilauea Volcano, Hawaii. *Bull. Volcanol.* **48**, 87–96.

GREELEY, R. & WOMER, M. B. 1981 Mare basin filling on the moon: Laboratory simulations. In *Proc. Lunar Planet. Sci. Conf.* vol. XII, pp. 651–663.

HALLWORTH, M. A., HUPPERT, H. E. & SPARKS, R. S. J. 1987 A laboratory simulation of basaltic lava flows. *Mod. Geol.* **11**, 93–107.

HODGSON, G. W. 1969 An experimental investigation of simulated lava flows using carbowax materials. M.S. thesis, Wright-Patterson A.F.B., Ohio, Air Force Inst. of Technology.

HOULT, D. P. 1972 Oil spreading on the sea. *Ann. Rev. Fluid Mech.* **4**, 341–368.

HULME, G. 1974 The interpretation of lava flow morphology. *Geophys. J. R. Astron. Soc.* **39**, 361–383.

HUPPERT, H. E. 1982 The propagation of two-dimensional and axisymmetric viscous gravity currents over a rigid horizontal surface. *J. Fluid Mech.* **121**, 43–58.

HUPPERT, H. E., SHEPHERD, J. B., SIGURDSSON, H. & SPARKS, R. S. J. 1982 On lava dome growth, with application to the 1979 lava extrusion of the Soufriere of St. Vincent. *J. Volcanol. Geotherm. Res.* **14**, 199–222.

HUPPERT, H. E. & SPARKS, R. S. J. 1988 Melting the roof of a chamber containing a hot, turbulently convecting fluid. *J. Fluid Mech.* **188**, 107–131.

MALIN, M. C. 1980 Lengths of Hawaiian lava flows. *Geology* **8**, 306–308.

MOORE, J. G. & LOCKWOOD, J. P. 1978 Spreading cracks on pillow lava. *J. Geol.* **86**, 661–671.

PARK, S. O. 1981 Simulation of lava flow with small scale models. Ph.D. thesis, Ames Iowa, Iowa State University, 173 pp.

PIERI, D. C. & BALOGA, S. M. 1986 Eruption rate, area, and length relationships for some Hawaiian lava flows. *J. Volcanol. Geotherm. Res.* **30**, 29–45.

PINKERTON, H. 1987 Factors affecting the morphology of lava flows. *Endeavour* **11**, 73–79.

PINKERTON, H. & SPARKS, R. S. J. 1978 Field measurements of the rheology of lava. *Nature* **276**, 383–386.

TEPLEY, L. & MOORE, J. G. 1974 Fire under the sea: The origin of pillow lava. 16 mm sound motion picture, Moonlight productions, Mountain View, Calif.

TURCOTTE, D. L. & SCHUBERT, G. 1982 *Geodynamics.* John Wiley.

TURNER, J. S. 1973 *Buoyancy Effects in Fluids.* Cambridge University Press.

WADGE, G. 1978 Effusion rate and the shape of aa lava flow-fields on Mount Etna. *Geology* **6**, 503–506.

WALKER, G. P. L. 1973 Lengths of lava flows. *Phil. Trans. R. Soc. Lond.* A **274**, 107–118.